Article

Cite This: Biomacromolecules 2018, 19, 2638−2649

pubs.acs.org/Biomac

Different-Length Hydrazone Activated Polymers for Plasmid DNA Condensation and Cellular Transfection

Juan M. Priegue,[†,§] Irene Lostalé-Seijo,[†,§] Daniel Crisan,[‡] Juan R. Granja,[†] Francisco Fernández-Trillo,[*,‡] and Javier Montenegro[*,†]

[†]Centro Singular de Investigación en Química Biolóxica e Materiais Moleculares (CIQUS), Departamento de Química Orgánica, Universidade de Santiago de Compostela, 15782 Santiago de Compostela, Spain

[‡]School of Chemistry, University of Birmingham, Birmingham B15 2TT, U.K.

Supporting Information

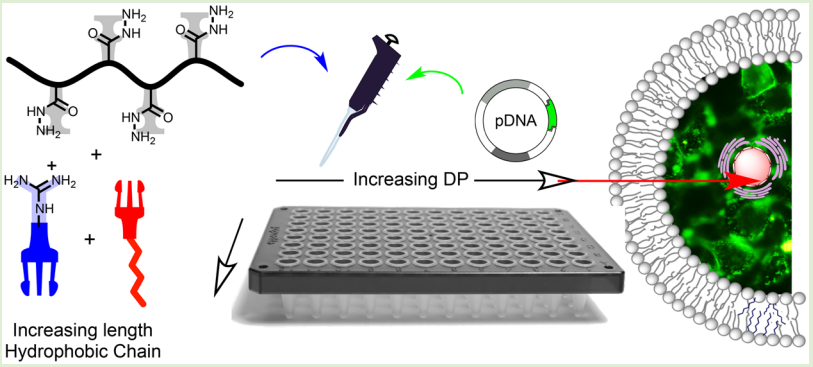

ABSTRACT: The recent advances in genetic engineering demand the development of conceptually new methods to prepare and identify efficient vectors for the intracellular delivery of different nucleotide payloads ranging from short single-stranded oligonucleotides to larger plasmid double-stranded circular DNAs. Although many challenges still have to be overcome, polymers hold great potential for intracellular nucleotide delivery and gene therapy. We here develop and apply the postpolymerization modification of polyhydrazide scaffolds, with different degree of polymerization, for the preparation of amphiphilic polymeric vehicles for the intracellular delivery of a circular plasmid DNA. The hydrazone formation reactions with a mixture of cationic and hydrophobic aldehydes proceed in physiologically compatible aqueous conditions, and the resulting amphiphilic polyhydrazones are directly combined with the biological cargo without any purification step. This methodology allowed the preparation of stable polyplexes with a suitable size and zeta potential to achieve an efficient encapsulation and intracellular delivery of the DNA cargo. Simple formulations that performed with efficiencies and cell viabilities comparable to the current gold standard were identified. Furthermore, the internalization mechanism was studied via internalization experiments in the presence of endocytic inhibitors and fluorescence microscopy. The results reported here confirmed that the polyhydrazone functionalization is a suitable strategy for the screening and identification of customized polymeric vehicles for the delivery of different nucleotide cargos.

INTRODUCTION

The transfection of genetic material to the interior of the cells continues to be a key challenge for chemical biology and biomaterials science.[1−10] Although great progress has been made in recent years, the potential of gene therapy remains fairly underexploited.[8] Thousands of clinical trials have been explored in the past decade, but only a few products have reached the market, including Gendicine in China, Glybera in the European Union, or the recently approved Luxturna in the United States.[4,6,8] Viral vectors still remain as one of the techniques of choice for cell transfection and gene therapy due to their efficacy and partial cellular selectivity.[1,11] However, the application of modified viral containers for gene delivery presents important problems such as the limited loading of viral capsids, the considerable immunogenic responses against viral proteins, the risk of fatal effects, and the ethical- and biosafety-related concerns.[1,6,11] These issues have prompted chemists, pharmacologists, and material scientists to develop synthetic vectors that could go beyond the current hurdles of nonviral vectors in the promising field of gene delivery.[5,6,12−14] Encouraging nucleic acid delivery properties have been explored for different molecules and materials such as lipids and lipidomimetics,[7,15−22] peptides,[23−47] supramolecular assemblies,[48−53] and polymers.[24,45,54−68] However, synthetic gene transporters still present several challenges such as the vector stability in physiological conditions, the frequent off-target

Received: February 12, 2018
Revised: April 10, 2018
Published: April 13, 2018

DOI: 10.1021/acs.biomac.8b00252
Biomacromolecules 2018, 19, 2638−2649

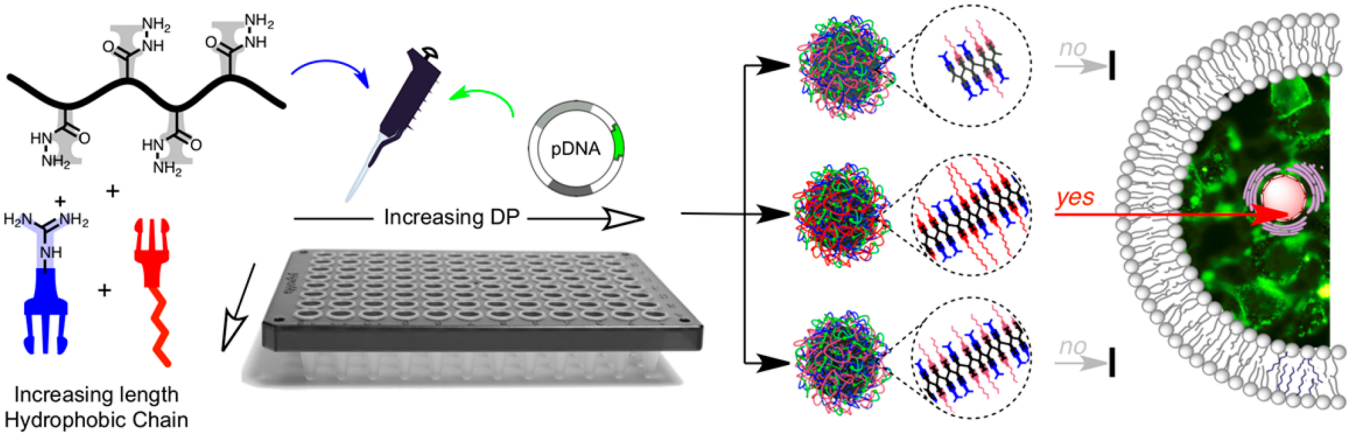

Figure 1. Schematic representation of screening of polyhydrazones for plasmid delivery. Polyhydrazides of different length (degree of polymerization − DP) were reacted with different combinations of a cationic and a hydrophobic aldehyde. The resulting amphiphilic activated polymers were incubated with a plasmid DNA encoding the green fluorescent protein (EGFP) to give rise to different polyplexes that were screened for gene delivery.

uptake, the high cytotoxicity, and the low activity in tissues and nondividing cells. Among the entire collection of nonviral vectors, polymers are of great interest as they can display multivalent chemical motifs required for cell transfection and can be easily produced in large scale. Therefore, different synthetic methodologies, including combinatorial strategies, have been explored to prepare polymers for DNA and RNA transfection.[54,59,69−71] However, standard polymerization reactions are normally carried out in the presence of organic solvents, and as a consequence, isolation and purification steps are always required before screening for biological activity. Furthermore, in most of these examples, the monomer composition strongly influences the final structure of the products after the polymerization reaction.[72,73] The hydrazone bio-orthogonal connection has been confirmed as an excellent and compatible chemical motif for the conjugation of chemical functions in different biomolecular templates.[31,74−80] In this regard, we have recently reported the use of the postpolymerization functionalization of polyhydrazide polymers to afford *in situ* activated amphiphilic polymers for the delivery of small interfering RNA (siRNA).[63] However, it is well-known that the intracellular nucleotide delivery mediated by synthetic nonviral vectors is strongly dependent on the nature and also the size of the transported cargo.[6,81]

Herein we report the development of the *in situ* generated polyhydrazone amphiphilic polymers for the delivery of a larger circular DNA plasmid in HeLa cells. In this work, we demonstrate the importance of the length of the polymer to accomplish the condensation and the delivery of nucleotides with different lengths. This was easily established thanks to the versatility of this methodology to screen different amphiphilic polymers that can be straightforwardly obtained in physiologically compatible conditions and without any isolation or purification steps. Polyhydrazides of different lengths were prepared and condensed with cationic and hydrophobic aldehydes to yield the corresponding amphiphilic polyhydrazones. These amphiphilic polymers were screened for the intracellular delivery of a plasmid DNA encoding the enhanced green fluorescent protein (EGFP). The results reported here highlight the adaptability of the strategy for the straightforward functionalization of polymer backbones in aqueous conditions and the potential application of the resulting polyhydrazones for the customized delivery of biological relevant molecules (Figure 1).

EXPERIMENTAL SECTION

Materials. Poly(acryloyl hydrazide) was synthesized according to our previously reported protocols[62,63] (see Supporting Information for full details and characterization). 2-((Ethylthio)carbonothioyl)thio-2-methylpropanoic acid (**CTA**) was synthesized according to protocols described in the literature[82] (see Supporting Information). The aldehydes tested were either commercially available or synthesized following reported protocols from the corresponding alcohols.[18,63]

Lipofectamine 2000 (LF), Penicillin−Streptomycin−Glutamine Mix, Trypsin-EDTA solution, and Dulbecco's Modified Eagle's Medium (4500 mg/L glucose, L-glutamine, sodium pyruvate, and sodium bicarbonate) were purchased from Fisher Scientific. Fetal bovine serum was purchased from Sigma-Aldrich. pEGFP-C1, a plasmid of 4731 bp encoding for the EGFP gene (see Figure S9), was obtained from Clontech. A 2.7 kb fluorescein labeled plasmid (Label IT Plasmid Delivery Control) was purchased from Mirus.

All other chemicals were purchased from Sigma-Aldrich, Fisher Scientific, VWR, or Acros, and used without further purification. All solvents were reagent grade or above; purchased from Sigma-Aldrich, Fisher Scientific, or VWR; and used without further purification.

Conjugation of Poly(acryloyl hydrazide) with Aldehyde Modulators. In a typical experiment, poly(acryloyl hydrazide) in acetate buffer (100 mM, pH 3.0) was reacted with 6 equiv of different molar fractions of guanidinium aldehyde ($\mathbf{T_1}$) and a hydrophobic aldehyde tail ($\mathbf{T_m}$). For most experiments, 25 μL of a solution of poly(acryloyl hydrazide) (37.2 mM, 15 μg/mL) in acetate buffer (100 mM, pH 3.0), 7.5 μL of a solution of $\mathbf{T_m}$ (223.2 mM) in dry DMSO, and 17.5 μL of a solution of $\mathbf{T_1}$ (223.2 mM) in dry DMSO were mixed to give a final $\mathbf{P_n}$ monomer concentration of 18.6 mM with a molar ratio $\chi\mathbf{T_1}$ = 0.70 and $\chi\mathbf{T_m}$ = 0.30. This mixture was shaken at 60 °C for 2 h. $\mathbf{P_nT_1}^{\chi}\mathbf{T_m}^{1-\chi}$ polymers were used without further purification for HeLa cells transfection experiments.

In Vitro Screening for Plasmid Delivery. HeLa cells were maintained in DMEM supplemented with 10% FBS and 1% Penicillin−Streptomycin−Glutamine Mix at 37 °C/5% CO_2/ 95% humidity. One day before transfection, cells were seeded in 96-well plates at a concentration of 50 000 cells/mL (100 μL/well).

Transfection was done by incubation of cells with 2.5 ng/μL of **pEGFP** and different concentrations (0.5−8 μg/mL) of the activated polymers ($\mathbf{P_nT_1}^{\chi}\mathbf{T_m}^{1-\chi}$). Activated polymers stock solutions were prepared in DMSO/acetate buffer (v/v) as described above, right before use. The solutions of $\mathbf{P_nT_1}^{\chi}\mathbf{T_m}^{1-\chi}$/**pEGFP** polyplexes were freshly prepared prior to the transfection experiments by mixing 10 μL of the **pEGFP** solution (50 ng/μL in DMEM) and 35 μL of

DOI: 10.1021/acs.biomac.8b00252
Biomacromolecules 2018, 19, 2638−2649

$\mathbf{P_nT_1}^{\chi}\mathbf{T_m}^{1-\chi}$ solution in DMEM for 30 min. After the incubation, the mixture was added to 155 μL of DMEM and homogenized by pipetting. Fifty microliters of this solution were added to each well of HeLa cells. Positive controls for transfection were prepared with Lipofectamine 2000 (6.6 μg/mL of Lipofectamine 2000 and 2.5 ng/μL **pEGFP**), and negative controls were untransfected cells and cells incubated with the same amount of plasmid in the absence of any carrier. After 4 h, transfection mixtures were replaced by 100 μL of DMEM supplemented with 10% FBS and antibiotics. The final concentration of DMSO in each well was 0.125% (v/v). All experiments were done in triplicate. EGFP expression was studied at 72 hpt by fluorometry, epifluorescence microscopy or flow cytometry.

Fluorometry. Three days after transfection, cell culture medium was replaced with PBS (137 mM NaCl, 2.7 mM KCl, 8 mM Na_2HPO_4, 1.5 mM KH_2PO_4) and EGFP expression measured by fluorometry in a Tecan Infinite F200Pro microplate reader (λ_{ex} 489 nm; λ_{em} 509 nm).

Epifluorescence Imaging of Transfected Cells. HeLa cells were transfected following the procedure described above. Cells were washed with PBS at 72 hpt and immediately imaged under the microscope.

Quantitation of the Number of Transfected Cells by Flow Cytometry. HeLa cells were transfected following the procedure described above. Three days after transfection, cells were washed with PBS, trypsinized with 100 μL of Trypsin-EDTA for 10 min at 37 °C, and trypsin was neutralized with 100 μL of 2% FBS in PBS with 5 mM EDTA. Cell clumps were broken by pipetting before analyzing on a Guava easyCyte cytometer. EGFP fluorescence was determined by excitation at 488 nm and detection at 512 nm/18 nm. Data analysis was performed with InCyte software included in GuavaSoft 3.2 (Millipore). For the analysis, cells with typical FSC and SSC parameters were selected, and cells were considered EGFP positive when fluorescence signal was higher than that of the untransfected cells. An increase in SSC and autofluorescence was observed for the cells incubated with the higher concentrations of the polymer/plasmid complexes, probably due to the remains of these complexes associated with the cell membrane, and it was taken into account for the gating (Figure S3).

Cell Viability: MTT Assay. Toxicity of the polyplexes was studied with a colorimetric MTT assay, in which metabolic activity of the cells causes the reduction of MTT to formazan. HeLa cells were transfected with the polyplexes prepared with different concentrations of the activated $\mathbf{P_nT_1}^{\chi}\mathbf{T_m}^{1-\chi}$ polymers (0.5−8 μg/mL) and 2.5 ng/μL of **pEGFP**. After 72 h of incubation, the medium was replaced by 100 μL of fresh medium supplemented with 10 μL of MTT (5 mg/mL stock solution in PBS), and further incubated for 4 h at 37 °C. The medium was carefully aspirated and the purple precipitate of formazan was dissolved with DMSO (100 μL/well). Absorbance at 570 nm was measured in a Tecan microplate reader. Values were normalized against untreated cells (100%).

Cellular Uptake Mechanisms. To study the mechanism of cellular uptake, HeLa cells growing in a 96 well plate were treated for 30 min with the following compounds diluted in DMEM without serum or antibiotics: Dynasore (80 μM), chlorpromazine (30 μM), methyl-β-cyclodextrin (5 mM), or EIPA (50 μM). For the incubation at low temperature, another plate was placed on ice, and ice-cold solutions were used for the washes and incubations. Cells were then incubated with 8 μg/mL of the $\mathbf{P_{80}T_1}^{0.7}\mathbf{T_5}^{0.3}$ polyplexes prepared with a fluorescein-labeled plasmid (2.5 ng/μL) in the presence of the same amount of inhibitors for 1 h at 37 °C. After the incubation, cells were washed twice with PBS and trypsinized. Trypsin was neutralized with 2% FBS in PBS containing 5 mM EDTA and cell-associated fluorescence was measured on a Guava EasyCyte cytometer using 488 nm excitation laser and detection at 512 nm/18 nm. Data analysis was done with InCyte software. Cells with typical FSC and SSC parameters were selected, and the median fluorescence intensity was calculated for each sample (MFI). Each condition was done in triplicate. Fluorescence values were normalized to the uptake of the untreated control (100%) after blank subtraction.

Epifluorescence Images of Transfection Complexes. HeLa cells were incubated with transfection complexes prepared with a plasmid labeled with fluorescein (2.5 ng/μL) and the $\mathbf{P_nT_1}^{0.7}\mathbf{T_5}^{0.3}$ (8 μg/mL) in DMEM without FBS. After 4 h of incubation, cells were washed and DMEM without phenol red supplemented with 10% FBS and 1% antibiotics was added. Cells were imaged at different times after the addition of the complexes using an epifluorescence microscope. To remove noninternalized complexes, another set of cells were washed at 1 or 6 hpt with a solution of 1 mg/mL heparin in PBS three times for 2 min each, before adding DMEM without phenol red supplemented with 10% FBS and 1% antibiotics and imaged (Figure S8).

Statistical Analysis. Statistical analysis was done with R-software.[83] Data was analyzed with pairwise Student's *t* test with Bonferroni's correction, and *p*-values <0.05 were considered significant.

Hydrodynamic Radius and ζ-Potential. Ten microliters of activated polymers stock solutions in DMSO/acetate buffer at different concentrations (8−2 μg/mL final concentration) were freshly mixed with a solution of **pEGFP** plasmid at a fixed concentration (2.5 ng/μL, 995 μL in water) and were incubated for 30 min before measuring. For the measurement of the polymers alone, 995 μL of plasmid solution was replaced by the same amount of bidistilled water. Bidistilled water was filtered through a membrane filter (0.45 μm) before use. Polyplex size and ζ-potential were determined using Malvern Zetasizer Nano ZS90. All experiments were done at 25 °C, and the mean values and standard deviations were obtained from triplicates.

Gel Retardation Assay. Freshly prepared $\mathbf{P_nT_1}^{0.7}\mathbf{T_5}^{0.3}$ were mixed in DMEM with **pEGFP** at different charge ratios (0.75, 1.5, 3, 6, 9 and 12) and incubated at room temperature for 30 min. The mixtures, including a solution of the free plasmid at the same concentration, were loaded into a 0.8% agarose gel containing 0.5 μg/mL ethidium bromide in TAE buffer (40 mM Tris, 20 mM acetic acid, and 1 mM EDTA). Electrophoresis was performed at 100 V for 15 min. Gels were imaged under UV light using a GelDoc system (Bio-Rad).

Atomic Force Microscopy (AFM). Standard AFM measurements were conducted in ambient atmosphere at room temperature in a Park Systems NX-10. ACTA tips were used (silicon tips, nominal values: spring constant = 40 N/m, frequency = 300 kHz, ROC less than 10 nm). Samples were prepared by incubating an 8 μg/mL solution of $\mathbf{P_{80}T_1}^{0.7}\mathbf{T_5}^{0.3}$ or $\mathbf{P_{180}T_1}^{0.7}\mathbf{T_5}^{0.3}$ with 2.5 ng/μL of **pEGFP** in Milli-Q water during 30 min. For AFM imaging, 30 μL of the sample was dropped onto freshly exfoliated mica, and after 15 min, the mica was thoroughly washed with Milli-Q water and dried under Argon Flow.

Sample Preparation for Electron Microscopy (TEM and STEM). Freshly prepared activated polymers $\mathbf{P_nT_1}^{0.7}\mathbf{T_5}^{0.3}$ were mixed with **pEGFP** (2.5 ng/μL) at a polymer concentration of 8 μg/mL in Milli-Q water. The mixture was incubated for 30 min and subsequently pipetted onto carbon coated copper grids. After 10 min, the remaining solution was removed with filter paper and thoroughly washed with ultrapure water. Samples were imaged without staining or after staining for 1 min with 10 μL of 2% phosphotungstic acid, followed by several washes with Milli-Q water. TEM images were acquired on a ZEISS Libra 200 FE Omega transmission electron microscope operating at 200 kV accelerating voltage. The same samples were measured by SEM and STEM on a Zeiss FESEM Ultra Plus.

RESULTS

Design and Initial Screening. We synthesized three poly(acryloyl hydrazides) with different degree of polymerization, namely **n** = 40, 80, and 180 ($\mathbf{P_{40}}$, $\mathbf{P_{80}}$ and $\mathbf{P_{180}}$, respectively). These polymers were prepared following the previously reported synthetic methodology as illustrated in Figure S1.[62,63] Briefly, the required monomer (*tert*-butyl-2-acryloylhydrazine-1-carboxylate) was prepared by standard acyl transfer protocols, and the monomer was polymerized by reversible addition−fragmentation (RAFT) polymerization and purified by dialysis against Milli-Q water.[63] Finally, the Boc-

DOI: 10.1021/acs.biomac.8b00252
Biomacromolecules 2018, 19, 2638−2649

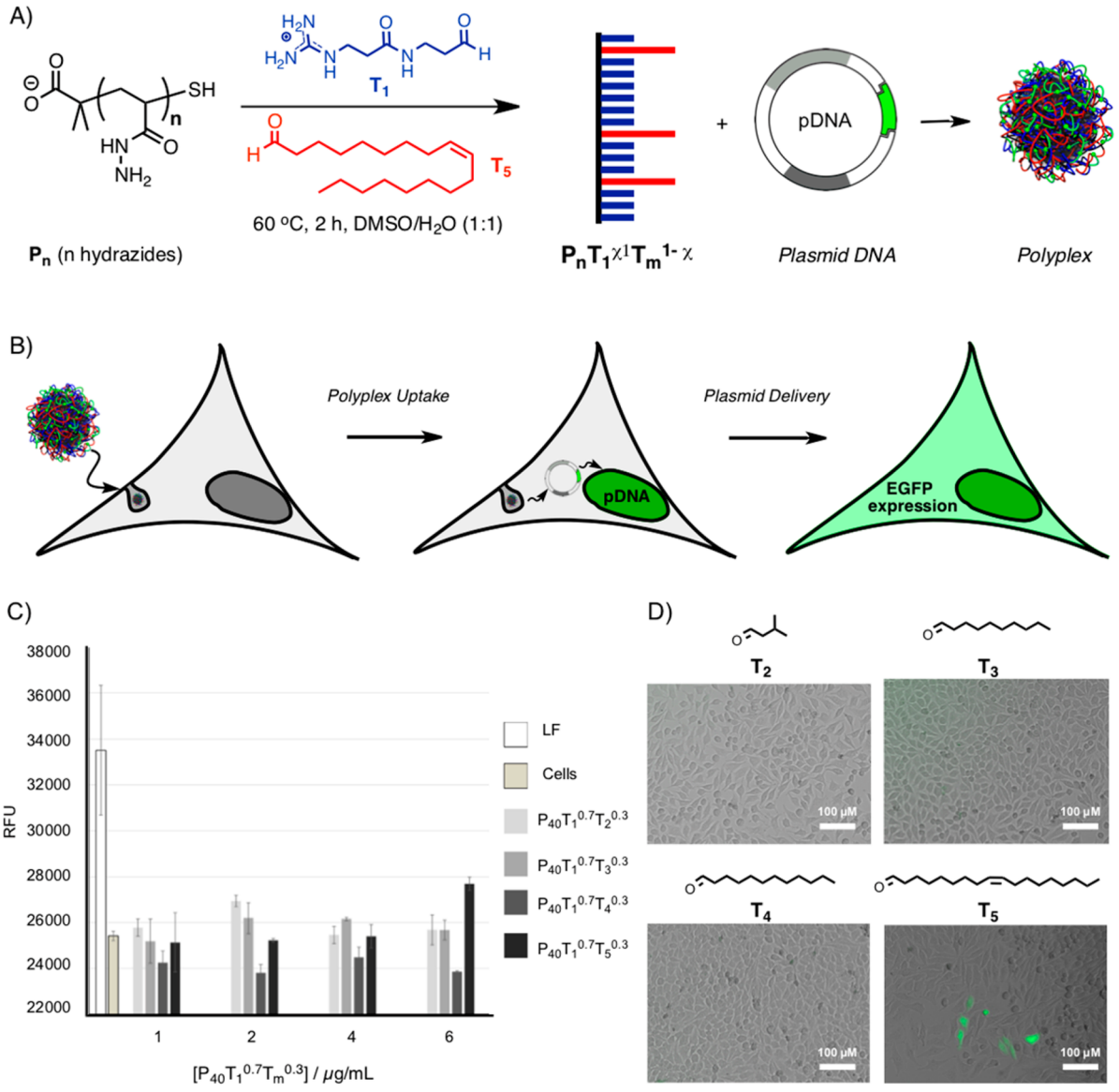

Figure 2. Polyhydrazone reaction, transfection scheme, and initial screening. (A) Schematic representation of polyplex formation through the reaction between the polymer with **n** hydrazides sites $\mathbf{P_n}$ with the cationic $\mathbf{T_1}$ and the hydrophobic $\mathbf{T_5}$ to afford the amphiphilic polyhydrazone $\mathbf{P_nT_1}^{\chi}\mathbf{T_5}^{1-\chi}$ that is then combined with the plasmid DNA for polyplex formation and analysis (the χ superindex corresponds to the molar fraction of the guanidinium aldehyde tail). (B) Scheme of the transfection experiments: after the uptake of the polyplex the DNA plasmid reaches the cell nucleus and the consequent expression of the enhanced green fluorescent protein (EGFP) can be quantified by fluorometry. (C) Relative fluorescence (λ_{ex} 489 nm; λ_{em} 509 nm) of HeLa cells transfected with $\mathbf{P_{40}}$ reacted with different hydrophobic tails, measured at 72 hpt. Lipofectamine (LF) was used as a positive control. Error bars indicate the standard deviation of three replicates. (D) Microscopy images of HeLa cells incubated with **pEGFP** and 6 μg/mL of $\mathbf{P_{40}T_1}^{0.7}\mathbf{T_m}^{0.3}$ at 72 hpt. The corresponding hydrophobic aldehydes are indicated above each panel.

protected polymers were treated with trifluoroacetic acid, neutralized with $NaHCO_3$, dialyzed against Milli-Q water, and lyophilized to afford the final polyhydrazides.[63] The full characterization of these polymers and corresponding polyhydrazones was carried out as described in our previous work.[62,63] The parent polyhydrazides were incubated with a mixture of one cationic and one hydrophobic aldehyde in H_2O/DMSO (1:1) at 60 °C. This incubation in aqueous conditions resulted in the corresponding amphiphilic polyhydrazones that could be combined *in situ* with the plasmid DNA without further purification (Figure 2A). As previously reported, we decided to fix the cationic moiety to the guanidinium derivative $\mathbf{T_1}$, as the pK_a of the guanidinium group (pK_a = 12.5) guarantees its protonation and thus cationic character at physiological pH.[51,84] To identify preliminary pairs of aldehydes suitable for further development, an initial screening of plasmid transfection in HeLa cells was performed using fluorometry to quantify transfection efficiency (Figure 2). We started evaluating similar conditions to the previously reported siRNA transport by reacting the shorter polymer ($\mathbf{P_{40}}$) with the guanidinium aldehyde ($\chi\mathbf{T_1}$ = 0.7) and four different hydrophobic aldehyde tails, namely, isovaleraldehyde, decanal, dodecanal, and oleic aldehyde ($\chi\mathbf{T_m}$ = 0.3). The corresponding activated polyhydrazone polymers were named as $\mathbf{P_nT_1}^{\chi}\mathbf{T_m}^{1-\chi}$, where **n** = degree of polymerization (DP) of the polyhydrazide used, **m** (2−5) is used to identify the hydrophobic aldehyde used, and χ is the molar fraction of the guanidinium aldehyde in the incubation mixture (Figure 2). Although an excess of

DOI: 10.1021/acs.biomac.8b00252
Biomacromolecules 2018, 19, 2638−2649

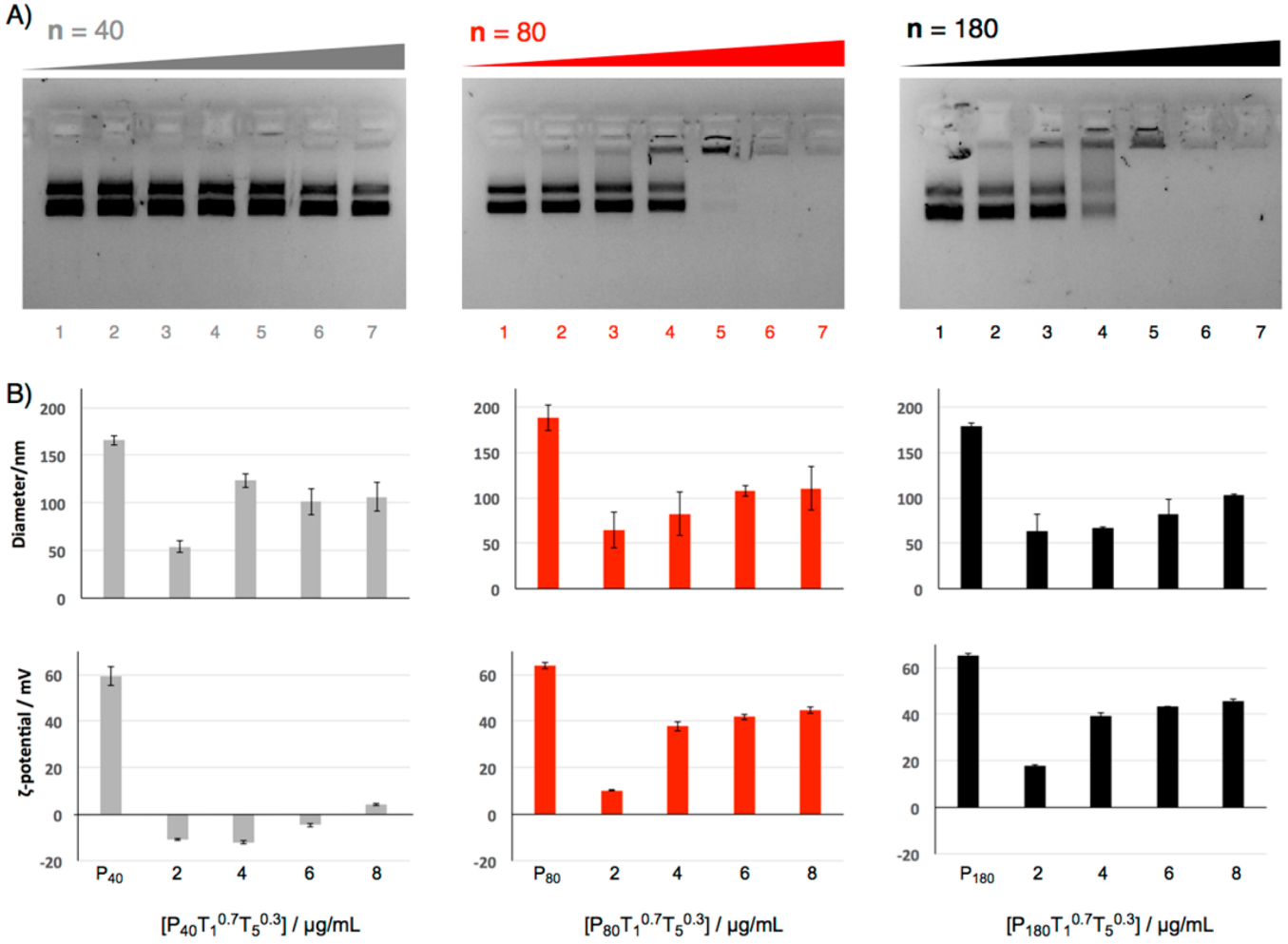

Figure 3. Gel retardation assay, DLS, and ζ-potential. (A) Gel retardation assay with the three polyhydrazones $\mathbf{P_nT_1}^{0.7}\mathbf{T_5}^{0.3}$. **pEGFP** (lane 1) and $\mathbf{P_nT_1}^{0.7}\mathbf{T_5}^{0.3}$/**pEGFP** polyplexes with different concentrations of polyhydrazones: 0.5 (lane 2), 1 (lane 3), 2 (lane 4), 4 (lane 5), 6 (lane 6), and 8 μg/mL (lane 7). [**pEGFP**] = 2.5 ng/μL. (B) Hydrodynamic diameter in nanometers (nm) by dynamic light scattering (DLS) and zeta potential (ζ) in millivolts (mV) of pure $\mathbf{P_nT_1}^{0.7}\mathbf{T_5}^{0.3}$ and $\mathbf{P_nT_1}^{0.7}\mathbf{T_5}^{0.3}$/**pEGFP** polyplexes at 2, 4, 6, and 8 μg/mL of polyhydrazone, measured in water. [**pEGFP**] = 2.5 ng/μL. Data is expressed as mean of triplicates; error bars indicate standard deviation.

aldehyde reactants was employed to maximize hydrazone formation, several control experiments have fully confirmed that aldehydes alone do not transfect cells.[18,40,42,63] After hydrazone formation, the amphiphilic polymer was incubated with the plasmid DNA in DMEM medium to form polyplexes via electrostatic interactions. The selected cargo (**pEGFP**) was a double-stranded circular plasmid DNA of 4.7 kilobases that includes promoter, EGFP coding sequence, polyadenylation sequences, and bacterial backbone (see supporting info).

In contrast to previous results observed for siRNA transfection where $\mathbf{P_{40}}$ polymer showed excellent transfection activity, these preliminary **pEGFP** delivery experiments revealed only traces of protein expression for the combination of $\mathbf{P_{40}}$ with the cationic $\mathbf{T_1}$ and the long unsaturated hydrophobic oleic aldehyde ($\mathbf{T_5}$, Figure 2C).[40,42] The poor transfection efficiency of the polyhydrazones derived from $\mathbf{P_{40}}$ combined with the larger DNA plasmid was confirmed by fluorescence micrographs, which showed a small number of green fluorescent cells 72 h post-transfection (Figure 2D).

DNA Complexation and Polyplex Formation. The low initial transfection efficiencies for $\mathbf{P_{40}}$ prompted us to further investigate in detail the impact of the polyhydrazide length for plasmid condensation and delivery. Based on the preliminary results with $\mathbf{P_{40}}$ (Figure 2C) and on previously reported successful examples for long unsaturated hydrophobic tails,[40,42] we decided to fix the hydrophobic tail to the oleic aldehyde for the subsequent optimization. Therefore, following described protocols,[62,63] $\mathbf{P_{40}}$, $\mathbf{P_{80}}$, and $\mathbf{P_{180}}$ were condensed with a fixed molar ratio of aldehydes of $\chi\mathbf{T_1}$ / $\chi\mathbf{T_5}$ = 0.7:0.3. After the reaction, the corresponding amphiphilic polyhydrazones were directly combined with the plasmid DNA, and the resulting polyplexes were studied by gel electrophoresis and dynamic light scattering (DLS) (Figure 3). As shown by the gel electrophoresis experiments, the shorter $\mathbf{P_{40}T_1}^{0.7}\mathbf{T_5}^{0.3}$ failed to complex the plasmid, whereas the medium and the longer polyhydrazones, $\mathbf{P_{80}T_1}^{0.7}\mathbf{T_5}^{0.3}$ and $\mathbf{P_{180}T_1}^{0.7}\mathbf{T_5}^{0.3}$, efficiently complexed the larger circular double-stranded DNA (Figure 3A). The DLS analysis of these amphiphilic polyhydrazones confirmed the formation of polyplexes with sizes between 70 and 100 nm (Figure 3B). The size and the zeta potential progressively increased with increasing concentrations of the polymers, and in agreement with the gel experiments, only the medium and the large polyhydrazones, $\mathbf{P_{80}T_1}^{0.7}\mathbf{T_5}^{0.3}$ and $\mathbf{P_{180}T_1}^{0.7}\mathbf{T_5}^{0.3}$, respectively, were able to afford polyplexes with the sufficient positive zeta potential of around 40 mV to stop DNA gel migration (Figure 3A,B).

DOI: 10.1021/acs.biomac.8b00252
Biomacromolecules 2018, 19, 2638−2649

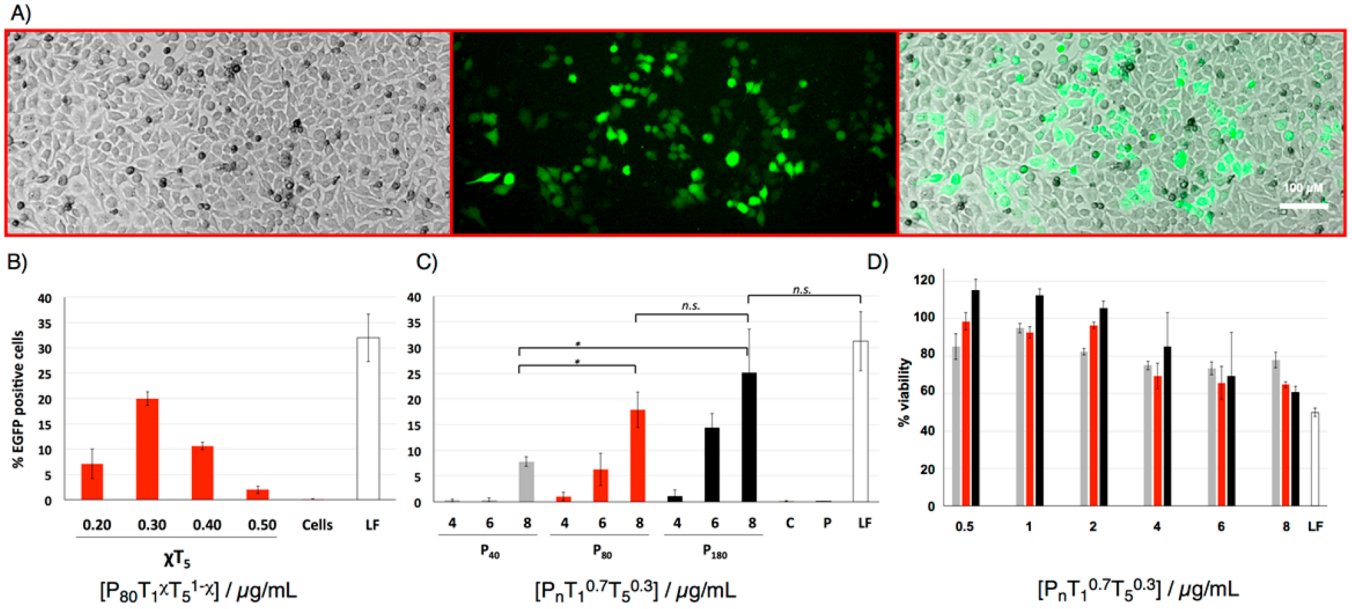

Figure 4. Transfection optimization and cell viability. (A) Bright-field images, green fluorescent channel and superimposed images of HeLa cells 3 days after transfection with polyplexes formed with 8 μg/mL of $\mathbf{P_{80}T_1^{0.7}T_5^{0.3}}$ and 2.5 ng/μL **pEGFP**. (B) Molar ratio optimization for the transfection of plasmid DNA (2.5 ng/μL) with $\mathbf{P_{80}T_1^{\chi}T_5^{1-\chi}}$ (8 μg/mL). Data is expressed as the mean of the percentage of transfected cells in three replicates. Error bars indicate standard deviation. (see also Figure S2). (C) Transfection efficiency of the polymers $\mathbf{P_{40}T_1^{0.7}T_5^{0.3}}$, $\mathbf{P_{80}T_1^{0.7}T_5^{0.3}}$, and $\mathbf{P_{180}T_1^{0.7}T_5^{0.3}}$ at different concentrations. **pEGFP** concentration was kept constant at 2.5 ng/μL. Data is expressed as the mean of the percentage of transfected cells in three independent transfection experiments. Error bars indicate standard deviation. The asterisk indicates a significant difference with a p-value of <0.05; n.s. indicates not significant (Student's t test with Bonferroni's correction) (see Figures S3 and S4). (D) MTT viability assay. HeLa cells were transfected with the indicated concentrations of the polymers $\mathbf{P_{40}T_1^{0.7}T_5^{0.3}}$ (gray bars), $\mathbf{P_{80}T_1^{0.7}T_5^{0.3}}$ (red bars) and $\mathbf{P_{180}T_1^{0.7}T_5^{0.3}}$ (black bars), and 2.5 ng/μL of plasmid, and 3 days after transfection, cell viability was measured with a MTT colorimetric assay. Values were normalized to untreated cells and expressed as mean and standard deviation of three replicates. In all cases, Lipofectamine 2000 (LF) was used at 6.6 μg/mL as recommended by the supplier.

Transfection Optimization and Cell Viability. Having confirmed the formation of polyplexes with a suitable size and zeta potential for the medium and longer polyhydrazides ($\mathbf{P_{80}}$ and $\mathbf{P_{180}}$), we next evaluated the **pEGFP** plasmid transfection ability of the three polymers in HeLa cells (Figure 4). In these experiments, the cells were incubated with the polyplexes resulting from the reaction of the three different polyhydrazides ($\mathbf{P_{40}}$, $\mathbf{P_{80}}$, and $\mathbf{P_{180}}$) with $\mathbf{T_1}$ and $\mathbf{T_5}$. We started by performing an optimization of the molar fraction of both aldehydes for the polymer $\mathbf{P_{80}}$ (Figure 4B), confirming the optimal cationic/hydrophobic molar fraction to be $\chi\mathbf{T_1}/\chi\mathbf{T_5}$ = 0.7:0.3 (Figure 4B), a value slightly higher than the previously reported for siRNA transfection.[63] With this fixed molar ratio, dose–response transfection experiments were carried out with increasing amounts of the three different amphiphilic polymers (Figure 4C). An increase in transfection efficiency with higher polymer concentrations was observed for the three polymers. As expected, the shorter polyhydrazone $\mathbf{P_{40}}$ that was not able to efficiently condense the DNA transfected less than 10% of the cells even at the highest concentration. Cytometry quantification of the transfection efficiency of the medium and the longer polyhydrazones ($\mathbf{P_{80}}$ and $\mathbf{P_{180}}$) showed significantly higher levels of efficacy than P40, above 20%, and at similar levels of transfection efficiency observed for the commercial vector Lipofectamine 2000 at a similar weight concentration (Figure 4C). Fluorescence microscopy images of cells transfected with the $\mathbf{P_{80}T_1^{0.7}T_5^{0.3}}$ polyhydrazone visually confirmed a good efficacy of the longer polymeric gene vector (Figure 4A). A dose–response MTT colorimetric assay was then carried out to study cell viability in the presence of the polyhydrazones at the working conditions of the transfection experiments (Figure 4D). These experiments established a slightly better cell viability and thus slightly lower toxicity for the transfecting polyhydrazones in comparison with the control with the Lipofectamine 2000 commercial vector.

Polyplex Microscopy Characterization. To further investigate the size and shape of the polyplexes, we performed a microscopic characterization of the transfecting polymer/plasmid nanostructures reported in this study (Figures 5, S5–S7). Nonstained scanning electron microscopy (SEM) micrographs on Formvar/carbon grids of the shorter polymer $\mathbf{P_{40}T_1^{0.7}T_5^{0.3}}$ polyplexes with **pEGFP** showed amorphous aggregated materials, an observation that sustained the poor transfection efficiency observed for this polymer length (Figure 2, Figure 4 and S3). This aggregation could indicate the lack of the required electrostatic repulsion between the complexes to stabilize individual particles. Analogous SEM micrographs for $\mathbf{P_{80}T_1^{0.7}T_5^{0.3}}$ and $\mathbf{P_{180}T_1^{0.7}T_5^{0.3}}$ combined with the plasmid DNA, showed particles of irregular globular shape, with a radius of around 40 nm (Figures 5C,D and S5). Atomic force microscopy (AFM) micrographs of $\mathbf{P_{80}T_1^{0.7}T_5^{0.3}}$ polyplexes deposited on mica surfaces showed particles with heights of around 20 nm (Figures 5B and S6). These low sizes obtained in AFM could be explained by a possible collapse of the cationic particles in the anionic mica surface, a situation that could cause the particle spreading over the hydrophilic surface employed for the atomic force microscopy. In an effort to clarify the differences in size from DLS and SEM, we acquired transmission electron microscopy (TEM) images after staining the fresh deposited sample with phosphotungstic acid followed

DOI: 10.1021/acs.biomac.8b00252
Biomacromolecules 2018, 19, 2638–2649

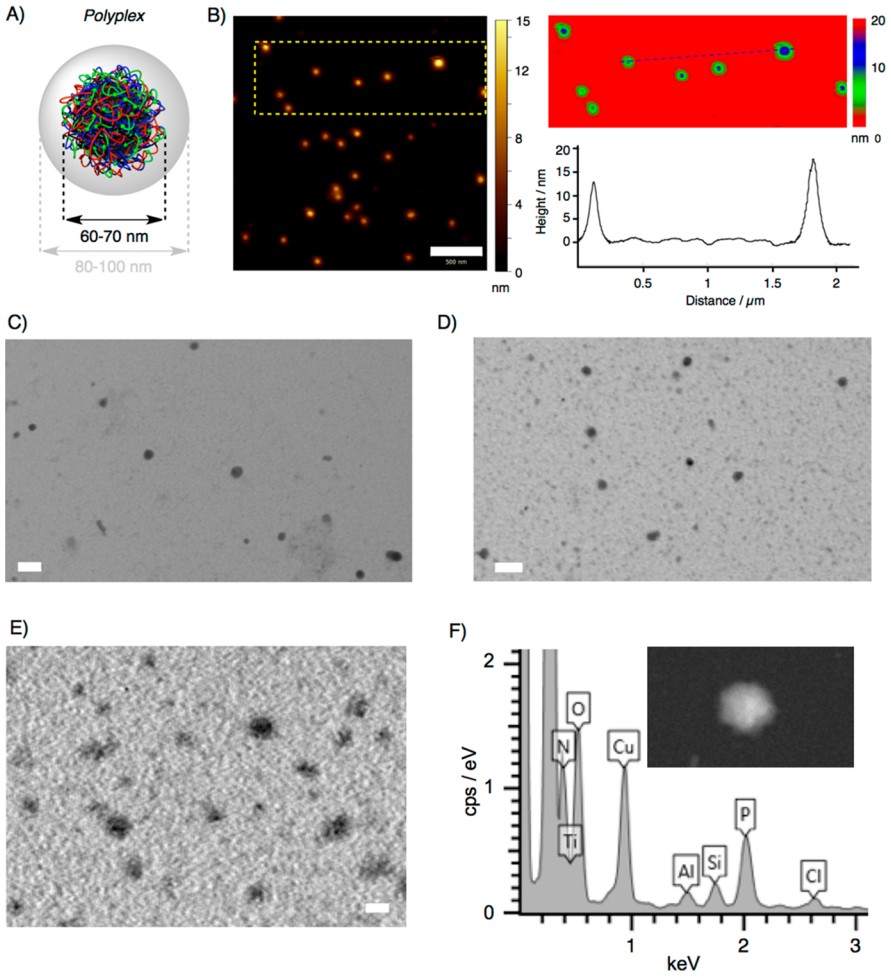

Figure 5. Characterization of the active polyplexes. (A) Scheme for the active polyplexes composed of the core of polymer/DNA complex observed in microscopy (~60−70 nm) that in the aqueous dispersion gives rise to bigger solvated suspended nanoparticles (80−100 nm). (B) AFM characterization of $\mathbf{P_{80}T_1^{0.7}T_5^{0.3}}$/ **pEGFP** deposited on mica surfaces. (C,D) Scanning electron microscopy (SEM) images of the polyplexes $\mathbf{P_{80}T_1^{0.7}T_5^{0.3}}$ / **pEGFP** (C) and $\mathbf{P_{180}T_1^{0.7}T_5^{0.3}}$ / **pEGFP** (D) deposited in electron microscopy grids. (E) Transmission electron microscopy (TEM) images $\mathbf{P_{180}T_1^{0.7}T_5^{0.3}}$ / **pEGFP** polyplexes deposited in electron microscopy grids and stained with of 2% phosphotungstic acid, followed by several washes with Milli-Q water. (F) Example of Scanning transmission electron micrograph (STEM) and energy-dispersive X-ray microanalysis depicting the presence of nitrogen (N) and phosphorus (P) in a polyplex of $\mathbf{P_{180}T_1^{0.7}T_5^{0.3}}$/ **pEGFP**. In Figure 5C−E, the scale bar is 100 nm. In all these cases, polyplexes were prepared in Milli-Q water.

by several washes of the microscopy grid with Milli-Q water. The stained images of the polyplexes from $\mathbf{P_{80}}$ and $\mathbf{P_{180}}$ polyhydrazones showed the presence of particles with higher diameters (~70 nm) and with irregular globular shape (Figures 5E and S7). The difference in size of the polyplexes obtained by electron microscopy (~70 nm) and DLS measurements (~90 nm) could be an effect of the desiccation and shrinkage of the polyplexes on the grid surface required for TEM studies, combined with the potential solvation sphere of the particles (Figures 3B and 5A).[85] Finally, scanning transmission electron microscopy (STEM) was carried out to investigate the polyplexes and confirm the presence of the DNA in the organic nanoparticles (Figure 5F). The energy-dispersive X-ray microanalysis of the nanoaggregates, prepared in Milli-Q water (see Experimental Section), confirmed the presence of nitrogen (N) and phosphorus (P) in the polyplexes of $\mathbf{P_{80}T_1^{0.7}T_5^{0.3}}$ and $\mathbf{P_{180}T_1^{0.7}T_5^{0.3}}$. The presence of these two atoms confirmed the condensation of the plasmid within the organic nanoparticles observed by electron microscopy.

Mechanistic Studies and Fluorescent Plasmid Tracking. We carried out transfection experiments with a fluorescently labeled plasmid (**CF-plasmid**, CF: carboxyfluorescein dye) to study the internalization mechanism of the polyplexes and to track the plasmid by fluorescence microscopy time-lapse images (Figure 6). In these experiments, the uptake of the **CF-plasmid** was quantified by flow cytometry in the presence or absence of endocytic inhibitors (Figure 6B). As expected for polyplexes of nanometric dimension and positive zeta potential, the uptake was strongly reduced at low temperature (4 °C), indicating an energy-dependent internalization pathway of the polyhydrazone/plasmid organic nanoparticles (Figure 6B). Dynasore, an inhibitor of macropinocytosis and all the internalization pathways that employ dynamin to release endosomes in the cytosol, reduced the polyplex uptake to a similar level as that obtained under low-temperature conditions (4 °C). Additionally, three inhibitors of specific endocytic mechanisms—chlorpromazine for clathrin-mediated endocytosis, methyl-β-cyclodextrin for caveolae mediated endocytosis, and EIPA for macropinocytosis—showed partial or strong inhibitory effects in the uptake of the polyplexes. All in all, these experiments suggested a macropinocytic route in combination with other endocytic

DOI: 10.1021/acs.biomac.8b00252
Biomacromolecules 2018, 19, 2638−2649

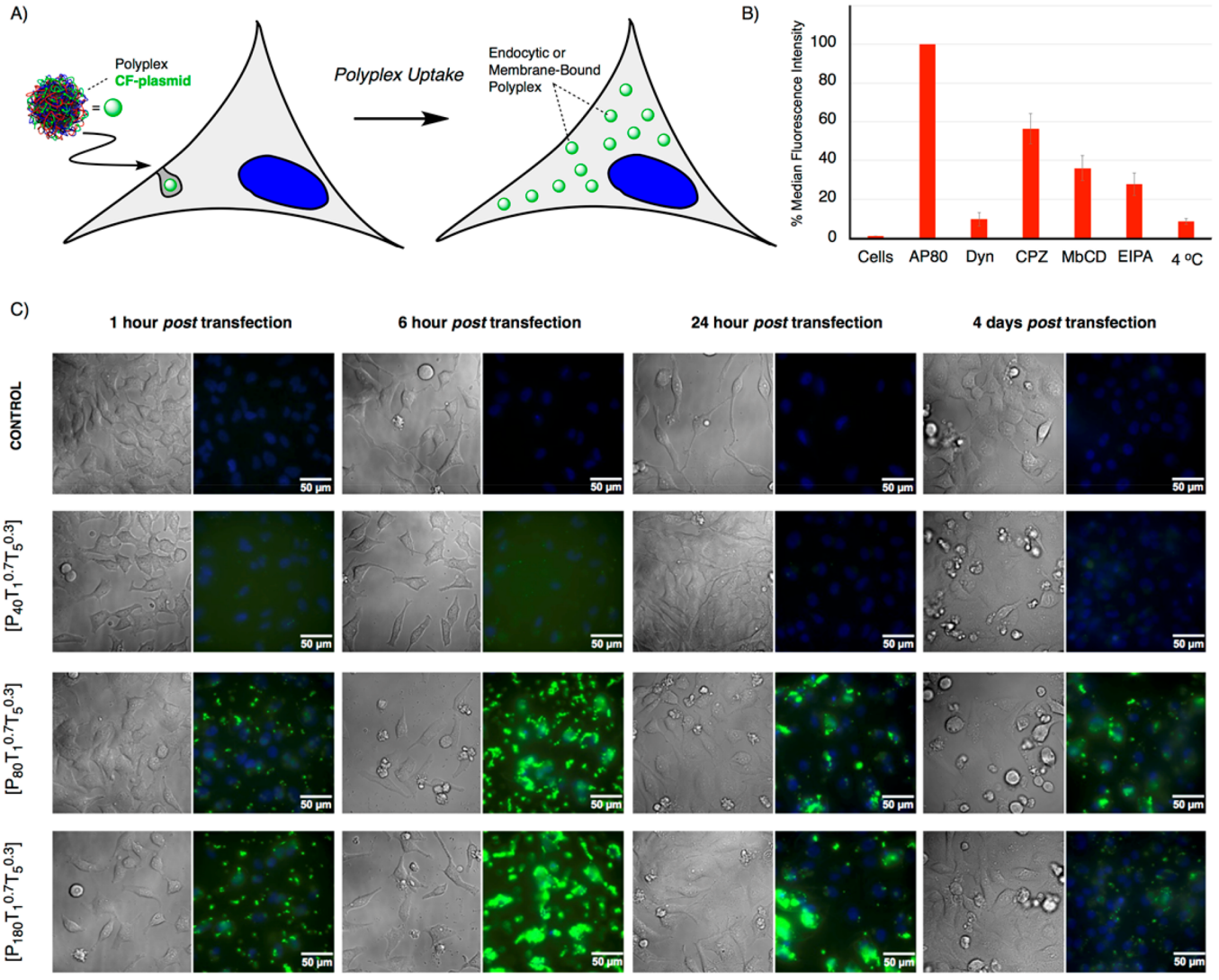

Figure 6. Uptake Mechanism and Plasmid Tracking. (A) Scheme for mechanistic studies. Polyplexes were prepared with a fluorescently labeled plasmid (**CF-plasmid**). (B) Polyplex internalization mechanism. HeLa cells were incubated with the polyplexes formed by **CF-plasmid** and $\mathbf{P_{80}T_1}^{0.7}\mathbf{T_5}^{0.3}$ in the absence or presence of endocytosis inhibitors and the uptake of the labeled plasmid was quantified by flow cytometry. Data is expressed as median fluorescence intensity normalized to the uptake of the polyplex by the untreated control (AP80), error bars indicate standard deviation of three replicates. (C) Time-lapse epifluorescence microscopy of the three polyplexes from the different-length polyhydrazones ($\mathbf{P_nT_1}^{0.7}\mathbf{T_5}^{0.3}$, **n** = 40, 80 and 180) with the fluorescently labeled **CF-plasmid** in HeLa cells. [$\mathbf{P_nT_1}^{0.7}\mathbf{T_5}^{0.3}$] = 8 μg/mL, [**CF-plasmid**] = 2.5 ng/μL. Cells were imaged at different times (1 and 6 hpt, 1 and 4 dpt). hpt: hours post-transfection, dpt: days post-transfection. Nuclei were counterstained with Hoechst (blue). See also Supporting Information.

mechanisms that could be operating at the same time for the uptake of the polyhydrazone/plasmid nanoparticles. We next carried out a fluorescence microscopy time-lapse experiment in cells to study internalization kinetics. In these experiments, the fluorescently labeled polyplexes were incubated with the cells for 4 h, carefully washed with medium, and further incubated in complete medium for microscopy analysis (Figures 6C and S8, see Supporting Information). The images showed a low level of membrane cellular attachment and a marginal signal of punctuated endosomes for the polyplexes made with $\mathbf{P_{40}T_1}^{0.7}\mathbf{T_5}^{0.3}$. However, the polyplexes of $\mathbf{P_{80}T_1}^{0.7}\mathbf{T_5}^{0.3}$ and $\mathbf{P_{180}T_1}^{0.7}\mathbf{T_5}^{0.3}$ showed a strong fluorescence signal located at the cell membrane level that increased until 6 h post transfection. As expected, the cellular punctate fluorescence signal from the endosomes was visible 1 h post-transfection. Intriguingly, this fluorescence signal was still present after 4 days, indicating that the polyplexes remained attached to the cell surface or internalized into endosomal compartments after long incubation times (Figure 6C). Analogous experiments were performed introducing extensive heparin washes to remove externally bound polyplexes. These experiments reduced the amount of fluorescent signal associated with the cells, indicating the presence of extracellular or membrane-bound particles, and showed that these polyplexes, in cell culture medium, tend to aggregate on the cell surface during the first hours (Figure S8).

DISCUSSION

The emergence of new techniques in gene therapy such as mRNA treatments, RNA interference, and genome editing demands the development of conceptually new methodologies for the nonviral transfection of different nucleotide cargos. The objective of this work was to demonstrate the versatility of the *in situ* modification of polymeric scaffolds[63] to deliver different nucleotide cargos inside cells. In particular, we wanted to

DOI: 10.1021/acs.biomac.8b00252
Biomacromolecules 2018, 19, 2638−2649

demonstrate that the recently reported methodology for the delivery of small siRNA[63] could be adapted to the more challenging delivery of plasmid DNA. In the latter application, the size of the nucleic acid is significantly increased; however, the delivery vehicle should be able to facilitate the transport of the desired cargo to the nuclei. For this purpose, in this work we synthesized polyhydrazides with different degree of polymerization that have been reacted with cationic and hydrophobic aldehydes to prepare the corresponding polyhydrazone amphiphiles. These activated polymers were combined with a DNA plasmid to study their capacity to complex the nucleic acid and produce stable polyplexes of suitable size and zeta potential for cell transfection. In contrast to previous results with siRNA,[63] we observed that short cationic amphiphilic polyhydrazones, derived from the polyhydrazide $\mathbf{P}_{40}$, were not able to complex the much larger plasmid anionic payload (Figure 2). This is in agreement with observations that suggest that for the delivery of plasmid DNA the formation of aggregates of an adequate size is critical for the uptake, while in the case of siRNA, due to its smaller size, the protection against enzymatic degradation is more important than condensation.[86] As a result of this lack of packing capacity, the shorter amphiphilic polymer could not efficiently translocate and deliver the lengthy nucleotide cargo across the cell membrane (Figures 2 and 3). However, the medium ($\mathbf{P}_{80}$) and long ($\mathbf{P}_{180}$) amphiphilic polyhydrazones, incorporating cationic ($\mathbf{T}_1$) and long hydrophobic ($\mathbf{T}_5$) pendants, efficiently packed and delivered the plasmid DNA inside living cells (Figure 4). These polyplexes showed good transfection efficiencies at a similar slightly lower range but with slightly better cell viabilities than the current gold standard for plasmid cell delivery, Lipofectamine 2000 (Figure 4). As previously observed for siRNA delivery with poly(ß)-amino esters and polyethylenimines,[6,81] the results reported here clearly highlight the importance of polymer length for plasmid transfection when carrying longer nucleotides payloads. Although an efficient nucleotide encapsulation constitutes a fundamental requirement for the packing and protection of the DNA cargo, the polyplex dissociation at the correct time and location constitutes the key step for an efficient delivery.[6] In this regard, it has been recently proposed that the release of individual polymers from the transported polyplexes could have important implications in the generation of escape routes for the endocytic nucleotide payloads.[61] The *in situ* modification of a parent polyhydrazide scaffold reported here offers a unique opportunity to screen for polymeric gene vectors, across a consistent degree of polymerization and with different functionalities that could have important implications in polyplex stability and thus cargo delivery. The mechanistic studies with endocytic inhibitors suggested that although macropinocytosis could be the main internalization pathway, several other endocytic mechanisms might be operating at the same time. However, the efficient plasmid expression observed for the polyplexes of $\mathbf{P}_{80}$ and $\mathbf{P}_{180}$ unmistakably demonstrated a release of the plasmid DNA from the endocytic vesicles and its arrival into the cell nuclei. Altogether, the excellent DNA packing capacity, the suitable transfection efficiency and cell viability confirmed the medium and larger polymers as suitable polymeric vehicles for the transfection of large anionic cargos.

CONCLUSIONS

In summary, in this work we have demonstrated the potential of hydrazone postpolymerization strategy to deliver plasmid DNAs inside human cells. The strategy allowed us to quickly extract important conclusions on the importance of the degree of polymerization for plasmid condensation and delivery. In contrast with the short siRNA (<25 base pairs), the larger plasmid DNA (>4500 base pairs) required a longer polymer for the efficient DNA condensation, membrane translocation, and nuclear delivery. The importance of this study builds on the versatility of the strategy to perform a straightforward screening and optimization of the polymer vector until the identification of the particular chemical and structural motifs required for the transport of a particular cargo. Therefore, the possibility of tuning the chemical properties of polymeric scaffolds with a consistent degree of polymerization constitutes an excellent alternative to identify potential customized vehicles for different cargos in a fully water-soluble and biocompatible methodology, which does not require any isolation or purification steps of the final compounds.

ASSOCIATED CONTENT

Supporting Information

The Supporting Information is available free of charge on the ACS Publications website at DOI: 10.1021/acs.biomac.8b00252.

Detailed information on the synthesis of the polymer, characterization of the chemical compounds, additional cell culture experiments, and electron microscopy images (PDF)

AUTHOR INFORMATION

Corresponding Authors

*E-mail: javier.montenegro@usc.es.
*E-mail: f.fernandez-trillo@bham.ac.uk.

ORCID

Juan R. Granja: 0000-0002-5842-7504
Francisco Fernández-Trillo: 0000-0002-6680-5683
Javier Montenegro: 0000-0001-6503-2095

Present Address

[⊥]National Institute of Material Physics, Atomistilor Str., No. 405A, 077125, Magurele, Ilfov, Romania.

Author Contributions

[§](J.M.P., I.L.-S.) These two authors contributed equally.

Notes

The authors declare no competing financial interest.

ACKNOWLEDGMENTS

We thank Dr. Iria Louzao for her kind assistance with the microscopy characterization. This work was partially supported by the Spanish Agencia Estatal de Investigación (AEI) [CTQ2014-59646-R, CTQ2016-78423-R, SAF2017-89890-R], the Xunta de Galicia (ED431G/09, ED431C 2017/25 and 2016-AD031), the ERDF, Royal Society U.K (IE130688 and RG140273), and the Wellcome Trust (177ISSFPP). J.M. received a Ramón y Cajal (RYC-2013-13784), an ERC Starting Investigator Grant (DYNAP-677786), and a Young Investigator Grant from the Human Frontier Science Research Program (RGY0066/2017). F. F.-T. thanks the Birmingham Science City and the European Regional Development Fund, and the University of Birmingham (John Evans Fellowship). J.M.P. thanks the Spanish Agencia Estatal de Investigación (AEI) for his research contract.

DOI: 10.1021/acs.biomac.8b00252
Biomacromolecules 2018, 19, 2638−2649

REFERENCES

(1) Thomas, C. E.; Ehrhardt, A.; Kay, M. A. Progress and Problems with the Use of Viral Vectors for Gene Therapy. *Nat. Rev. Genet.* **2003**, *4* (5), 346−358.

(2) Kostarelos, K.; Miller, A. Synthetic, Self-Assembly ABCD Nanoparticles; a Structural Paradigm for Viable Synthetic Non-Viral Vectors. *Chem. Soc. Rev.* **2005**, *34* (11), 970−994.

(3) Mintzer, M. A.; Simanek, E. E. Nonviral Vectors for Gene Delivery. *Chem. Rev.* **2009**, *109* (2), 259−302.

(4) Sheridan, C. Gene Therapy Finds Its Niche. *Nat. Biotechnol.* **2011**, *29* (2), 121−128.

(5) Zhang, Y.; Satterlee, A.; Huang, L. In Vivo Gene Delivery by Nonviral Vectors: Overcoming Hurdles? *Mol. Ther.* **2012**, *20* (7), 1298−1304.

(6) Yin, H.; Kanasty, R. L.; Eltoukhy, A. A.; Vegas, A. J.; Dorkin, J. R.; Anderson, D. G. Non-Viral Vectors for Gene-Based Therapy. *Nat. Rev. Genet.* **2014**, *15* (8), 541−555.

(7) Safinya, C. R.; Ewert, K. K.; Majzoub, R. N.; Leal, C. Cationic Liposome−Nucleic Acid Complexes for Gene Delivery and Gene Silencing. *New J. Chem.* **2014**, *38*, 5164−5172.

(8) Hill, A. B.; Chen, M.; Chen, C.-K.; Pfeifer, B. A.; Jones, C. H. Overcoming Gene-Delivery Hurdles: Physiological Considerations for Nonviral Vectors. *Trends Biotechnol.* **2016**, *34* (2), 91−105.

(9) Zhang, P.; Wagner, E. History of Polymeric Gene Delivery Systems. *Top. Curr. Chem.* **2017**, *375* (2), 26−39.

(10) Wong, J. K. L.; Mohseni, R.; Hamidieh, A. A.; MacLaren, R. E.; Habib, N.; Seifalian, A. M. Will Nanotechnology Bring New Hope for Gene Delivery? *Trends Biotechnol.* **2017**, *35* (5), 434−451.

(11) Kotterman, M. A.; Schaffer, D. V. Engineering Adeno-Associated Viruses for Clinical Gene Therapy. *Nat. Rev. Genet.* **2014**, *15* (7), 445−451.

(12) Guo, X.; Huang, L. Recent Advances in Nonviral Vectors for Gene Delivery. *Acc. Chem. Res.* **2012**, *45* (7), 971−979.

(13) Bechara, C. R.; Sagan, S. Cell-Penetrating Peptides: 20 years Later, Where Do We Stand? *FEBS Lett.* **2013**, *587* (12), 1693−1702.

(14) Malamas, A. S.; Gujrati, M.; Kummitha, C. M.; Xu, R.; Lu, Z.-R. Design and evaluation of new pH-sensitive amphiphilic cationic lipids for siRNA delivery. *J. Controlled Release* **2013**, *171* (3), 296−307.

(15) Xu, Y.; Szoka, F. Mechanism of DNA Release From Cationic Liposome/DNA Complexes Used in Cell Transfection. *Biochemistry* **1996**, *35* (18), 5616−5623.

(16) Koltover, I.; Salditt, T.; Rädler, J. O.; Safinya, C. R. An Inverted Hexagonal Phase of Cationic Liposome-DNA Complexes Related to DNA Release and Delivery. *Science* **1998**, *281* (5373), 78−81.

(17) Martin, B.; Sainlos, M.; Aissaoui, A.; Oudrhiri, N.; Hauchecorne, M.; Vigneron, J. P.; Lehn, J. M.; Lehn, P. The Design of Cationic Lipids for Gene Delivery. *Curr. Pharm. Des.* **2005**, *11* (3), 375−394.

(18) Gehin, C.; Montenegro, J.; Bang, E.-K.; Cajaraville, A.; Takayama, S.; Hirose, H.; Futaki, S.; Matile, S.; Riezman, H. Dynamic Amphiphile Libraries to Screen for the "Fragrant" Delivery of siRNA Into HeLa Cells and Human Primary Fibroblasts. *J. Am. Chem. Soc.* **2013**, *135* (25), 9295−9298.

(19) Kohli, A. G.; Kierstead, P. H.; Venditto, V. J.; Walsh, C. L.; Szoka, F. C. Designer lipids for drug delivery: From heads to tails. *J. Controlled Release* **2014**, *190* (C), 274−287.

(20) Colombani, T.; Peuziat, P.; Dallet, L.; Haudebourg, T.; Mével, M.; Berchel, M.; Lambert, O.; Habrant, D.; Pitard, B. Self-Assembling Complexes Between Binary Mixtures of Lipids with Different Linkers and Nucleic Acids Promote Universal mRNA, DNA and siRNA Delivery. *J. Controlled Release* **2017**, *249* (C), 131−142.

(21) Copolovici, D. M.; Langel, K.; Eriste, E.; Langel, Ü. Cell-Penetrating Peptides: Design, Synthesis, and Applications. *ACS Nano* **2014**, *8* (3), 1972−1994.

(22) Yang, J.; Bahreman, A.; Daudey, G.; Bussmann, J.; Olsthoorn, R. C. L.; Kros, A. Drug Delivery via Cell Membrane Fusion Using Lipopeptide Modified Liposomes. *ACS Cent. Sci.* **2016**, *2* (9), 621−630.

(23) Morris, M. C.; Depollier, J.; Mery, J.; Heitz, F.; Divita, G. A Peptide Carrier for the Delivery of Biologically Active Proteins Into Mammalian Cells. *Nat. Biotechnol.* **2001**, *19* (12), 1173−1176.

(24) Astriab-Fisher, A.; Sergueev, D.; Fisher, M.; Shaw, B. R.; Juliano, R. L. Conjugates of Antisense Oligonucleotides with the Tat and Antennapedia Cell-Penetrating Peptides: Effects on Cellular Uptake, Binding to Target Sequences, and Biologic Actions. Pharm. *Pharm. Res.* **2002**, *19* (6), 744−754.

(25) Li, W.; Nicol, F.; Szoka, F. C. GALA: a Designed Synthetic pH-Responsive Amphipathic Peptide with Applications in Drug and Gene Delivery. *Adv. Drug Delivery Rev.* **2004**, *56* (7), 967−985.

(26) Wadia, J. S.; Stan, R. V.; Dowdy, S. F. Transducible TAT-HA Fusogenic Peptide Enhances Escape of TAT-Fusion Proteins After Lipid Raft Macropinocytosis. *Nat. Med.* **2004**, *10* (3), 310−315.

(27) Meade, B. R.; Dowdy, S. F. Enhancing the Cellular Uptake of siRNA Duplexes Following Noncovalent Packaging with Protein Transduction Domain Peptides. *Adv. Drug Delivery Rev.* **2008**, *60* (4−5), 530−536.

(28) Palm-Apergi, C.; Lönn, P.; Dowdy, S. F. Do Cell-Penetrating Peptides Actually "Penetrate" Cellular Membranes? *Mol. Ther.* **2012**, *20* (4), 695−697.

(29) Koren, E.; Torchilin, V. P. Cell-Penetrating Peptides: Breaking Through to the Other Side. *Trends Mol. Med.* **2012**, *18* (7), 385−393.

(30) Stanzl, E. G.; Trantow, B. M.; Vargas, J. R.; Wender, P. A. Fifteen Years of Cell-Penetrating, Guanidinium-Rich Molecular Transporters: Basic Science, Research Tools, and Clinical Applications. *Acc. Chem. Res.* **2013**, *46* (12), 2944−2954.

(31) Montenegro, J.; Bang, E.-K.; Sakai, N.; Matile, S. Synthesis of an Enlarged Library of Dynamic DNA Activators with Oxime, Disulfide and Hydrazone Bridges. *Chem. - Eur. J.* **2012**, *18* (33), 10436−10443.

(32) Nakase, I.; Akita, H.; Kogure, K.; Gräslund, A.; Langel, Ü.; Harashima, H.; Futaki, S. Efficient Intracellular Delivery of Nucleic Acid Pharmaceuticals Using Cell-Penetrating Peptides. *Acc. Chem. Res.* **2012**, *45* (7), 1132−1139.

(33) Lindberg, S.; Regberg, J.; Eriksson, J.; Helmfors, H.; Muñoz Alarcón, A.; Srimanee, A.; Figueroa, R. A.; Hallberg, E.; Ezzat, K.; Langel, Ü. A Convergent Uptake Route for Peptide- and Polymer-Based Nucleotide Delivery Systems. *J. Controlled Release* **2015**, *206* (C), 58−66.

(34) More, H. T.; Frezzo, J. A.; Dai, J.; Yamano, S.; Montclare, J. K. Gene Delivery from Supercharged Coiled-coil Protein and Cationic Lipid Hybrid Complex. *Biomaterials* **2014**, *35* (25), 7188−7193.

(35) Priegue, J. M.; Montenegro, J.; Granja, J. R. Single-Nucleotide-Resolution DNA Differentiation by Pattern Generation in Lipid Bilayer Membranes. *Small* **2014**, *10* (18), 3613−3618.

(36) Li, M.; Schlesiger, S.; Knauer, S. K.; Schmuck, C. A Tailor-Made Specific Anion-Binding Motif in the Side Chain Transforms a Tetrapeptide Into an Efficient Vector for Gene Delivery. *Angew. Chem., Int. Ed.* **2015**, *54* (10), 2941−2944.

(37) Akishiba, M.; Takeuchi, T.; Kawaguchi, Y.; Sakamoto, K.; Yu, H.-H.; Nakase, I.; Takatani-Nakase, T.; Madani, F.; Gräslund, A.; Futaki, S. Cytosolic Antibody Delivery by Lipid-Sensitiveendosomolytic Peptide. *Nat. Chem.* **2017**, *9* (8), 751−761.

(38) Herce, H. D.; Schumacher, D.; Schneider, A. F. L.; Ludwig, A. K.; Mann, F. A.; Fillies, M.; Kasper, M.-A.; Reinke, S.; Krause, E.; Leonhardt, H.; Cardoso, M. C.; Hackenberger, C. P. R. Cell-Permeable Nanobodies for Targetedimmunolabelling and Antigen Manipulation In Living Cells. *Nat. Chem.* **2017**, *9* (8), 762−771.

(39) Kalafatovic, D.; Giralt, E. Cell-Penetrating Peptides: Design Strategies Beyond Primary Structure and Amphipathicity. *Molecules* **2017**, *22* (11), 1929.

(40) Louzao, I.; García-Fandiño, R.; Montenegro, J. Hydrazone-Modulated Peptides for Efficient Gene Transfection. *J. Mater. Chem. B* **2017**, *5*, 4426−4434.

(41) Pazo, M.; Fernández-Caro, H.; Priegue, J. M.; Lostalé-Seijo, I.; Montenegro, J. Tuning the Properties of Penetrating Peptides by Oxime Conjugation. *Synlett* **2017**, *28*, 924−928.

DOI: 10.1021/acs.biomac.8b00252
Biomacromolecules 2018, 19, 2638−2649

(42) Lostalé-Seijo, I.; Louzao, I.; Juanes, M.; Montenegro, J. Peptide/Cas9 Nanostructures for Ribonucleoprotein Cell Membrane Transport and Gene Edition. *Chem. Sci.* **2017**, *8*, 7923−7931.
(43) Meng, Z.; Luan, L.; Kang, Z.; Feng, S.; Meng, Q.; Liu, K. Histidine-enriched multifunctional peptide vectors with enhanced cellular uptake and endosomal escape for gene delivery. *J. Mater. Chem. B* **2017**, *5*, 74−84.
(44) Bai, Y.; Nguyen, L.; Song, Z.; Peng, S.; Lee, J.; Zheng, N.; Kapoor, I.; Hagler, L. D.; Cai, K.; Cheng, J.; Chan, H. Y. E.; Zimmerman, S. C. Integrating Display and Delivery Functionality with a Cell Penetrating Peptide Mimic as a Scaffold for Intracellular Multivalent Multitargeting. *J. Am. Chem. Soc.* **2016**, *138* (30), 9498−9507.
(45) Sgolastra, F.; deRonde, B. M.; Sarapas, J. M.; Som, A.; Tew, G. N. Designing Mimics of Membrane Active Proteins. *Acc. Chem. Res.* **2013**, *46* (12), 2977−2987.
(46) Lönn, P.; Kacsinta, A. D.; Cui, X.-S.; Hamil, A. S.; Kaulich, M.; Gogoi, K.; Dowdy, S. F. Enhancing Endosomal Escape for Intracellular Delivery of Macromolecular Biologic Therapeutics. *Sci. Rep.* **2016**, *6*, 32301.
(47) Boisguerin, P.; Deshayes, S.; Gait, M. J.; O'Donovan, L.; Godfrey, C.; Betts, C. A.; Wood, M. J. A.; Lebleu, B. Delivery of Therapeutic Oligonucleotides with Cell Penetrating Peptides. *Adv. Drug Delivery Rev.* **2015**, *87* (C), 52−67.
(48) Sigwalt, D.; Holler, M.; Iehl, J.; Nierengarten, J.-F.; Nothisen, M.; Morin, E.; Remy, J.-S. Gene Delivery with Polycationic Fullerene Hexakis-Adducts. *Chem. Commun.* **2011**, *47* (16), 4640−4642.
(49) Dahlman, J. E.; Barnes, C.; Khan, O. F.; Thiriot, A.; Jhunjunwala, S.; Shaw, T. E.; Xing, Y.; Sager, H. B.; Sahay, G.; Speciner, L.; Bader, A.; Bogorad, R. L.; Yin, H.; Racie, T.; Dong, Y.; Jiang, S.; Seedorf, D.; Dave, A.; Sandhu, K. S.; Webber, M. J.; Novobrantseva, T.; Ruda, V. M.; Lytton-Jean, A. K. R.; Levins, C. G.; Kalish, B.; Mudge, D. K.; Perez, M.; Abezgauz, L.; Dutta, P.; Smith, L.; Charisse, K.; Kieran, M. W.; Fitzgerald, K.; Nahrendorf, M.; Danino, D.; Tuder, R. M.; von Andrian, U. H.; Akinc, A.; Panigrahy, D.; Schroeder, A.; Koteliansky, V.; Langer, R.; Anderson, D. G. In Vivo Endothelial siRNA Delivery Using Polymeric Nanoparticles with Low Molecular Weight. *Nat. Nanotechnol.* **2014**, *9* (8), 648−655.
(50) Bartolami, E.; Bessin, Y.; Bettache, N.; Gary-Bobo, M.; Garcia, M.; Dumy, P.; Ulrich, S. Multivalent DNA Recognition by Self-Assembled Clusters: Deciphering Structural Effects by Fragments Screening and Evaluation as siRNA Vectors. *Org. Biomol. Chem.* **2015**, *13* (36), 9427−9438.
(51) Gasparini, G.; Bang, E.-K.; Montenegro, J.; Matile, S. Cellular Uptake: Lessons From Supramolecular Organic Chemistry. *Chem. Commun.* **2015**, *51* (52), 10389−10402.
(52) Bartolami, E.; Bouillon, C.; Dumy, P.; Ulrich, S. Bioactive Clusters Promoting Cell Penetration and Nucleic Acid Complexation for Drug and Gene Delivery Applications: From Designed to Self-Assembled and Responsive Systems. *Chem. Commun.* **2016**, *52*, 4257−4273.
(53) Fuertes, A.; Juanes, M.; Granja, J. R.; Montenegro, J. Supramolecular Functional Assemblies: Dynamic Membrane Transporters and Peptide Nanotubular Composites. *Chem. Commun.* **2017**, *53*, 7861−7871.
(54) Boussif, O.; Lezoualc'h, F.; Zanta, M. A.; Mergny, M. D.; Scherman, D.; Demeneix, B.; Behr, J. P. A Versatile Vector for Gene and Oligonucleotide Transfer Into Cells in Culture and in Vivo: Polyethylenimine. *Proc. Natl. Acad. Sci. U. S. A.* **1995**, *92* (16), 7297−7301.
(55) Barua, S.; Joshi, A.; Banerjee, A.; Matthews, D.; Sharfstein, S. T.; Cramer, S. M.; Kane, R. S.; Rege, K. Parallel Synthesis and Screening of Polymers for Nonviral Gene Delivery. *Mol. Pharmaceutics* **2009**, *6* (1), 86−97.
(56) Davis, M. E. The First Targeted Delivery of siRNA in Humans via a Self-Assembling, Cyclodextrin Polymer-Based Nanoparticle: From Concept to Clinic. *Mol. Pharmaceutics* **2009**, *6* (3), 659−668.
(57) Wang, H.; Liu, K.; Chen, K.-J.; Lu, Y.; Wang, S.; Lin, W.-Y.; Guo, F.; Kamei, K.-I.; Chen, Y.-C.; Ohashi, M.; Wang, M.; Garcia, M. A.; Zhao, X.-Z.; Shen, C. K.-F.; Tseng, H.-R. A Rapid Pathway Toward a Superb Gene Delivery System: Programming Structural and Functional Diversity Into a Supramolecular Nanoparticle Library. *ACS Nano* **2010**, *4* (10), 6235−6243.
(58) Kim, T.-I.; Rothmund, T.; Kissel, T.; Kim, S. W. Bioreducible Polymers with Cell Penetrating and Endosome Buffering Functionality for Gene Delivery Systems. *J. Controlled Release* **2011**, *152* (1), 110−119.
(59) Wagner, E. Polymers for siRNA Delivery: Inspired by Viruses to Be Targeted, Dynamic, and Precise. *Acc. Chem. Res.* **2012**, *45* (7), 1005−1013.
(60) Nakayama, Y. Hyperbranched Polymeric "Star Vectors" for Effective DNA or siRNA Delivery. *Acc. Chem. Res.* **2012**, *45* (7), 994−1004.
(61) Vaidyanathan, S.; Orr, B. G.; Banaszak Holl, M. M. Role of Cell Membrane−Vector Interactions in Successful Gene Delivery. *Acc. Chem. Res.* **2016**, *49* (8), 1486−1493.
(62) Crisan, D. N.; Creese, O.; Ball, R.; Brioso, J. L.; Martyn, B.; Montenegro, J.; Fernandez-Trillo, F. Poly(Acryloyl Hydrazide), a Versatile Scaffold for the Preparation of Functional Polymers: Synthesis and Post-Polymerisation Modification. *Polym. Chem.* **2017**, *8* (31), 4576−4584.
(63) Priegue, J. M.; Crisan, D. N.; Martínez-Costas, J.; Granja, J. R.; Fernandez-Trillo, F.; Montenegro, J. In Situ Functionalized Polymers for siRNA Delivery. *Angew. Chem., Int. Ed.* **2016**, *55* (26), 7492−7495.
(64) Dhande, Y. K.; Wagh, B. S.; Hall, B. C.; Sprouse, D.; Hackett, P. B.; Reineke, T. M. N-Acetylgalactosamine Block- Co-Polycations Form Stable Polyplexes with Plasmids and Promote Liver-Targeted Delivery. *Biomacromolecules* **2016**, *17* (3), 830−840.
(65) Zong, L.; Bartolami, E.; Abegg, D.; Adibekian, A.; Sakai, N.; Matile, S. Epidithiodiketopiperazines: Strain-Promoted Thiol-Mediated Cellular Uptake at the Highest Tension. *ACS Cent. Sci.* **2017**, *3* (5), 449−453.
(66) Abegg, D.; Gasparini, G.; Hoch, D. G.; Shuster, A.; Bartolami, E.; Matile, S.; Adibekian, A. Strained Cyclic Disulfides Enable Cellular Uptake by Reacting with the Transferrin Receptor. *J. Am. Chem. Soc.* **2017**, *139* (1), 231−238.
(67) Yan, Y.; Xiong, H.; Zhang, X.; Cheng, Q.; Siegwart, D. J. Systemic mRNA Delivery to the Lungs by Functional Polyester-Based Carriers. *Biomacromolecules* **2017**, *18* (12), 4307−4315.
(68) McKinlay, C. J.; Vargas, J. R.; Blake, T. R.; Hardy, J. W.; Kanada, M.; Contag, C. H.; Wender, P. A.; Waymouth, R. M. Charge-Altering Releasable Transporters (CARTs) for the Delivery and Release of mRNA in Living Animals. *Proc. Natl. Acad. Sci. U. S. A.* **2017**, *114* (4), E448−E456.
(69) Siegwart, D. J.; Whitehead, K. A.; Nuhn, L.; Sahay, G.; Cheng, H.; Jiang, S.; Ma, M.; Lytton-Jean, A.; Vegas, A.; Fenton, P.; Levins, C. G.; Love, K. T.; Lee, H.; Cortez, C.; Collins, S. P.; Li, Y. F.; Jang, J.; Querbes, W.; Zurenko, C.; Novobrantseva, T.; Langer, R.; Anderson, D. G. Combinatorial Synthesis of Chemically Diverse Core-Shell Nanoparticles for Intracellular Delivery. *Proc. Natl. Acad. Sci. U. S. A.* **2011**, *108* (32), 12996−13001.
(70) Hao, J.; Kos, P.; Zhou, K.; Miller, J. B.; Xue, L.; Yan, Y.; Xiong, H.; Elkassih, S.; Siegwart, D. J. Rapid Synthesis of a Lipocationic Polyester Library via Ring-Opening Polymerization of Functional Valerolactones for Efficacious siRNA Delivery. *J. Am. Chem. Soc.* **2015**, *137* (29), 9206−9209.
(71) Cheng, Y.; Sellers, D. L.; Tan, J.-K. Y.; Peeler, D. J.; Horner, P. J.; Pun, S. H. Development of Switchable Polymers to Address the Dilemma of Stability and Cargo Release in Polycationic Nucleic Acid Carriers. *Biomaterials* **2017**, *127*, 89−96.
(72) Lynn, D. M.; Anderson, D. G.; Putnam, D.; Langer, R. Accelerated Discovery of Synthetic Transfection Vectors: Parallel Synthesis and Screening of a Degradable Polymer Library. *J. Am. Chem. Soc.* **2001**, *123* (33), 8155−8156.
(73) Akinc, A.; Lynn, D. M.; Anderson, D. G.; Langer, R. Parallel Synthesis and Biophysical Characterization of a Degradable Polymer Library for Gene Delivery. *J. Am. Chem. Soc.* **2003**, *125* (18), 5316−5323.

DOI: 10.1021/acs.biomac.8b00252
Biomacromolecules 2018, 19, 2638−2649

(74) Montenegro, J.; Fin, A.; Matile, S. Comprehensive Screening of Octopus Amphiphiles as DNA Activators in Lipid Bilayers: Implications on Transport, Sensing and Cellular Uptake. *Org. Biomol. Chem.* **2011**, *9* (8), 2641−2647.
(75) Whitaker, D. E.; Mahon, C. S.; Fulton, D. A. Thermoresponsive Dynamic Covalent Single-Chain Polymer Nanoparticles Reversibly Transform Into a Hydrogel. *Angew. Chem., Int. Ed.* **2013**, *52* (3), 956−959.
(76) Wu, Z.; Chen, K.; Yildiz, I.; Dirksen, A.; Fischer, R.; Dawson, P. E.; Steinmetz, N. F. Development of Viral Nanoparticles for Efficient Intracellular Delivery. *Nanoscale* **2012**, *4* (11), 3567−3576.
(77) Tatum, L. A.; Su, X.; Aprahamian, I. Simple Hydrazone Building Blocks for Complicated Functional Materials. *Acc. Chem. Res.* **2014**, *47* (7), 2141−2149.
(78) Lehn, J. M. Perspectives in Chemistry-Aspects of Adaptive Chemistry and Materials. *Angew. Chem., Int. Ed.* **2015**, *54* (11), 3276−3289.
(79) Herrmann, A. Dynamic Mixtures: Challenges and Opportunities for the Amplification and Sensing of Scents. *Chem. - Eur. J.* **2012**, *18* (28), 8568−8577.
(80) Herrmann, A. Dynamic Combinatorial/Covalent Chemistry: a Tool to Read, Generate and Modulate the Bioactivity of Compounds and Compound Mixtures. *Chem. Soc. Rev.* **2014**, *43* (6), 1899−1933.
(81) Eltoukhy, A. A.; Siegwart, D. J.; Alabi, C. A.; Rajan, J. S.; Langer, R.; Anderson, D. G. Effect of Molecular Weight of Amine End-Modified Poly(β-Amino Ester)S on Gene Delivery Efficiency and Toxicity. *Biomaterials* **2012**, *33* (13), 3594−3603.
(82) Skey, J.; O'Reilly, R. K. Facile One Pot Synthesis of a Range of Reversible Addition−Fragmentation Chain Transfer (RAFT) Agents. *Chem. Commun.* **2008**, *31* (35), 4183−4183.
(83) R Core Team. *R: a Language and Environment for Statistical Computing*; R Foundation for Statistical Computing: Vienna, Austria, 2015.
(84) Montenegro, J.; Gehin, C.; Bang, E.-K.; Fin, A.; Doval, D. A.; Riezman, H.; Sakai, N.; Matile, S. Conceptually New Entries Into Cells. *Chimia* **2011**, *65* (11), 853−858.
(85) Hühn, J.; Carrillo-Carrion, C.; Soliman, M. G.; Pfeiffer, C.; Valdeperez, D.; Masood, A.; Chakraborty, I.; Zhu, L.; Gallego, M.; Yue, Z.; Carril, M.; Feliu, N.; Escudero, A.; Alkilany, A. M.; Pelaz, B.; del Pino, P.; Parak, W. J. Selected Standard Protocols for the Synthesis, Phase Transfer, and Characterization of Inorganic Colloidal Nanoparticles. *Chem. Mater.* **2017**, *29* (1), 399−461.
(86) Wang, T.; Upponi, J. R.; Torchilin, V. P. Design of multifunctional non-viral gene vectors to overcome physiological barriers: dilemmas and strategies. *Int. J. Pharm.* **2012**, *427* (1), 3−20.

DOI: 10.1021/acs.biomac.8b00252
Biomacromolecules 2018, 19, 2638−2649